Smart Structures and Systems, *Vol. 30, No. 4 (2022) 371-383*
https://doi.org/10.12989/sss.2022.30.4.371

Impact localization method for composite structures subjected to temperature fluctuations

Rahim Gorgin* and Ziping Wang [a]

Faculty of Civil Engineering and Mechanics, Jiangsu University, Zhenjiang 212013, Jiangsu, China

(*Received January 6, 2022, Revised June 20, 2022, Accepted July 7, 2022*)

Abstract. A novel impact localization method is presented based on impact induced elastic waves in sensorized composite structure subjected to temperature fluctuations. In real practices, environmental and operational conditions influence the acquired signals and consequently make the feature (particularly Time of Arrival (TOA)) extraction process, complicated and troublesome. To overcome this complication, a robust TOA estimation method is proposed based on the times in which the absolute amplitude of the signal reaches to a specific amplitude value. The presented method requires prior knowledge about the normalized wave velocity in different directions of propagation. To this aim, a finite element model of the plate was built in ABAQUS/CAE. The impact location is then highlighted by calculating an error value at different points of the structure. The efficiency of the developed impact localization technique is experimentally evaluated by dropping steel balls with different energies on a carbon fiber composite plate with different temperatures. It is demonstrated that the developed technique is able to localize impacts with different energies even in the presence of noise and temperature fluctuations.

Keywords: composite plate; elastic waves; impact localization; piezoelectric transducer; temperature fluctuations

1. Introduction

Impact events such as bird strikes, hailstone, and debris are of major concern for composite aircraft structures. Such type of impacts can generate visually undetectable damage in composite structures which may grow in the structure, leading to a detriment of mechanical properties with possible catastrophic failure during service (Farrar and Worden 2006, Gorgin *et al*. 2015, Zhong and Xiang 2019). Therefore, impact location identification and resultant damage characterization in aircraft composite structures is very important.

Upon impact, elastic waves are generated into composite plates and can be captured using piezoelectric (PZT) sensors (Qiu *et al*. 2018). Several passive impact location identification techniques have been developed using these collected signals.

Primary methods were based on the triangulation technique where the impact location is highlighted using the linear relation between Time of Arrival (TOA) of the wave and the relative distance travelled to each sensor (Coverley and Staszewski 2003). However, these primary methods were limited to isotropic and homogeneous structures of known wave velocity. Kundu *et al*. (2007, 2008) proposed a technique based on the minimization of an error function, which is able to highlight impact location in isotropic and anisotropic structures. However, their proposed technique required the determination of the wave velocity in different directions. To tackle this efficiency, Ciampa and Meo (2010a) developed a modification of the triangulation technique in isotropic materials, which did not require the knowledge of the wave velocity. Ciampa *et al*. (2012) proposed a technique for impact localization in anisotropic plates of unknown mechanical properties and wave velocity direction dependency. In addition, De Simone and Ciampa (De Simone *et al*. 2017) proposed a technique capable of highlighting the impact location in isotropic and anisotropic structures, with no requirement for known velocity profile.

Another technique based on the knowledge of the wave velocity is the beamforming method, which was originally proposed by McLaskey *et al*. (2010) and was later used by He *et al*. (2012). This technique is based on the delay-and-sum algorithm. Nakatani *et al*. (2013) extended this method to composite structures with requirement for pre-calculation of the wave velocity.

The main issue of such impact location identification methods is the estimation of the time of arrival (TOA) with high level of accuracy. Several approaches were used in the past for TOA estimation. Ciampa and Meo (2010b) proposed a technique based on the magnitude of the squared modulus of the Continuous Wavelet Transform (CWT). However, CWT strongly depends on the selection of the mother wavelet, which may limit its use for structures with complex geometries. Other techniques for the TOA estimation include fractal dimension (Boschetti *et al*. 1996), cross-correlation (Ziola and Gorman 1991, Kosel *et al*. 2003), spectrograms (Xu 2011), and the Hinkley criterion (Hinkley 1971).

All of these TOA estimation methods require signal processing and interpretation of the signal. Particularly,

*Corresponding author, Ph.D.,
E-mail: rgorgin@ujs.edu.cn
[a] Ph.D.

ISSN: 1738-1584 (Print), 1738-1991 (Online)

because in real practices, signals can be affected by environmental and operational conditions (Huynh and Kim 2016, Seno and Aliabadi 2019, Gorgin *et al*. 2020, Gorgin and Wang 2021, Seno and Aliabadi 2022). This limits their application in real-time impact location identification techniques.

The other impact localization techniques are the data driven techniques. These methods include the database reference methods (Park *et al*. 2012, Kim *et al*. 2015, Jang and Kim 2016, Shrestha *et al*. 2017, Zhao *et al*. 2018) and machine learning methods (Sharif Khodaei *et al*. 2012, Jang *et al*. 2012, Yue and Sharif Khodaei 2016, Jang and Kim 2019). These methods require an initial reference set of signals which can be impossible to store especially for huge structures such as aircrafts.

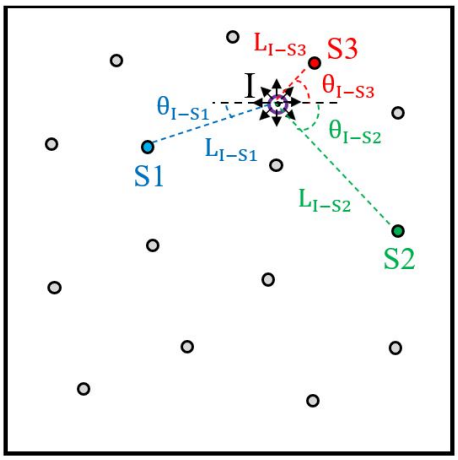

Fig. 1 A sensorized composite plate

In order to tackle these obstacles, the goal of this paper is to propose an impact localization method for composite structures which not only doesn't need any reference set of signals, also it doesn't require the interpretation of the collected signals. The presented method requires the approximate time of arrivals and the wave velocities in all directions of propagation. Hence, a TOA estimation technique is developed based on the time in which the amplitude of a signal reaches to a specific amplitude. Then, a simple finite element analysis is used to determine the normalized wave velocities in all directions of propagation. Finally, the structure is meshed into uniformly grid points and for each grid point an error value is calculated. The grid point with the minimum error value highlights the location of impact. The efficiency of the developed technique is checked by dropping a steel ball with different energies on a carbon fiber composite plate. It is demonstrated that the presented technique can highlight the location of impacts even in presence of noise and temperature fluctuations.

2. Methodology

Consider the sensorized composite plate shown in Fig. 1. Impact induced elastic waves can be acquired by

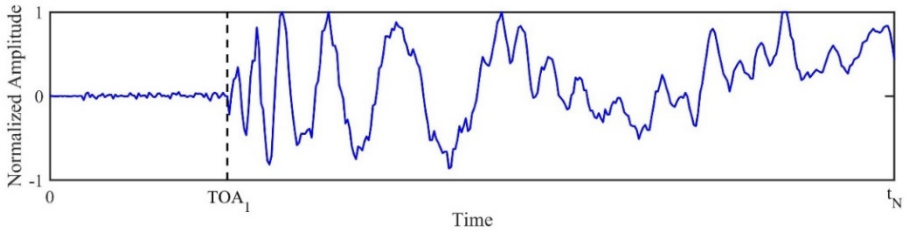

(a) S1

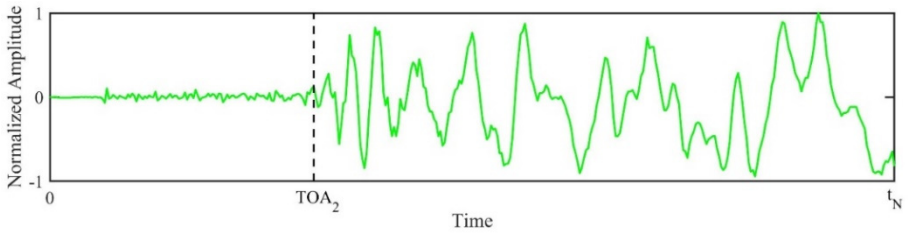

(b) S2

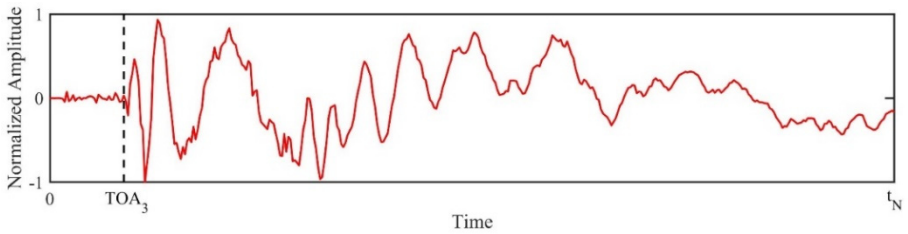

(c) S3

Fig. 2 Typical signal collected by sensor

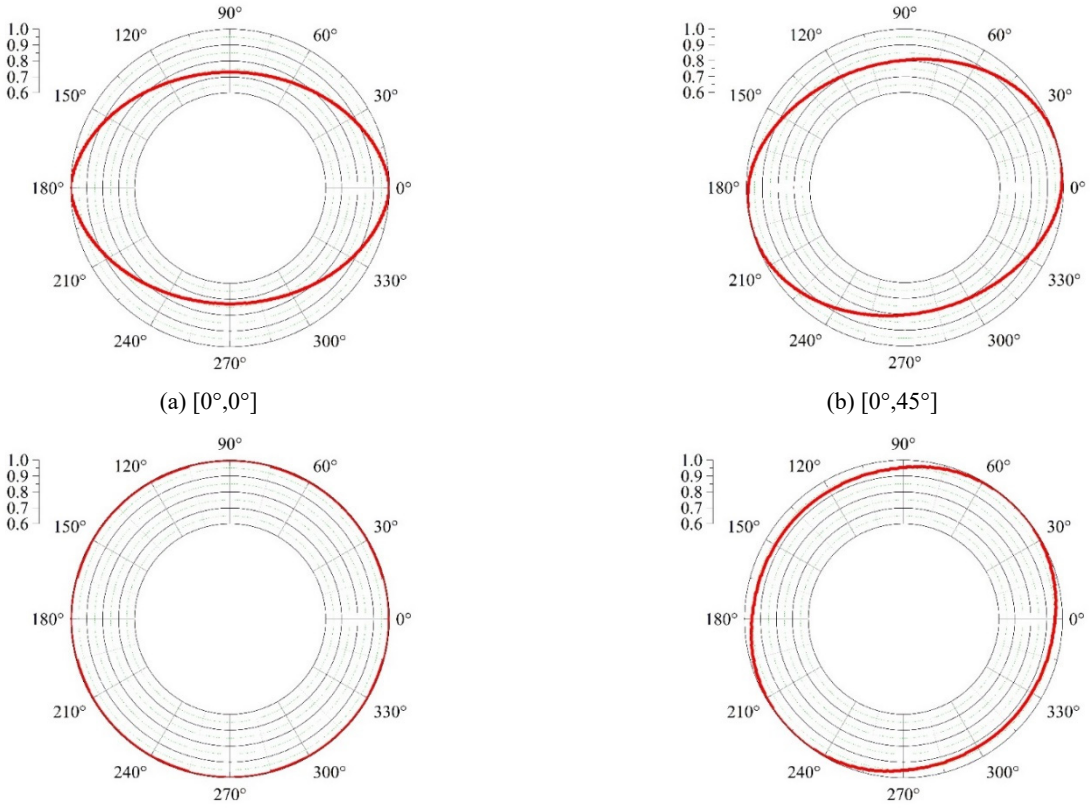

(a) [0°,0°] (b) [0°,45°]

(c) [-45°,45°] (d) [0°,45°,90°]

Fig. 3 — Normalized velocity of elastic waves in different directions of composite plates

distributed sensors. For example, Fig. 2 shows signals collected by sensors S1, S2, and S3 which are respectively located at distances $L_{\text{I-S1}}$, $L_{\text{I-S2}}$, $L_{\text{I-S3}}$, and angles $\theta_{\text{I-S1}}$, $\theta_{\text{I-S2}}$, and $\theta_{\text{I-S3}}$ with respect to the impact point I.

We can write

$$L_{\text{I-S1}} = V_{\theta_{\text{I-S1}}} \times \text{TOA}_1 \tag{1a}$$

$$L_{\text{I-S2}} = V_{\theta_{\text{I-S2}}} \times \text{TOA}_2 \tag{1b}$$

$$L_{\text{I-S3}} = V_{\theta_{\text{I-S3}}} \times \text{TOA}_3 \tag{1c}$$

where, $V_{\theta_{\text{I-S1}}}$, $V_{\theta_{\text{I-S2}}}$, and $V_{\theta_{\text{I-S3}}}$are the velocity and TOA_1, TOA_2, and TOA_3 are the time of arrivals of elastic waves respectively in path I-S1, I-S2, and I-S3.

In real practices, the signal features (such as velocity and time of arrival) are affected by environmental and operational conditions, particularly temperature fluctuations.

However, if we consider a uniform temperature change in the whole structure, the influence of temperature fluctuation on collected signals can be compensated by dividing two similar features from two different signals.

For instance, based on Eq. (1) it can be written

$$\frac{L_{\text{I-S1}}}{L_{\text{I-S2}}} = \frac{V_{\theta_{\text{I-S1}}}}{V_{\theta_{\text{I-S2}}}} \times \frac{\text{TOA}_1}{\text{TOA}_2} \tag{2a}$$

$$\frac{L_{\text{I-S1}}}{L_{\text{I-S3}}} = \frac{V_{\theta_{\text{I-S1}}}}{V_{\theta_{\text{I-S3}}}} \times \frac{\text{TOA}_1}{\text{TOA}_3} \tag{2b}$$

$$\frac{L_{\text{I-S2}}}{L_{\text{I-S3}}} = \frac{V_{\theta_{\text{I-S2}}}}{V_{\theta_{\text{I-S3}}}} \times \frac{\text{TOA}_2}{\text{TOA}_3} \tag{2c}$$

In this way, while due to temperature fluctuations the velocity and time of arrival of each signal may be changed, the ratio of velocities and time of arrivals approximately remains constant.

In order to use Eq. (2) for impact localization, first of all, the velocity of elastic waves in all directions need to be determined. To achieve this, finite element analysis can be used. Since, in Eq. (2), the ratio of velocities is appeared, therefore the normalized wave velocities can be used. For instance, Fig. 3 demonstrates the normalized wave velocity at different directions of typical carbon fibre composite plates.

Moreover, the time of arrival of each signal needs to be estimated. To this aim, a novel TOA estimation method is developed based on the times at which the amplitude of a signal reaches a specific amplitude.

Since, the material properties of the composite plates in different directions are different, the amplitude of elastic waves at different directions is different. For example, Fig. 4, demonstrates the normalized amplitude of waves at different directions of typical carbon fiber composite plates.

Furthermore, composite plates have high attenuation ratio. Therefore, the first step for TOAs prediction is to

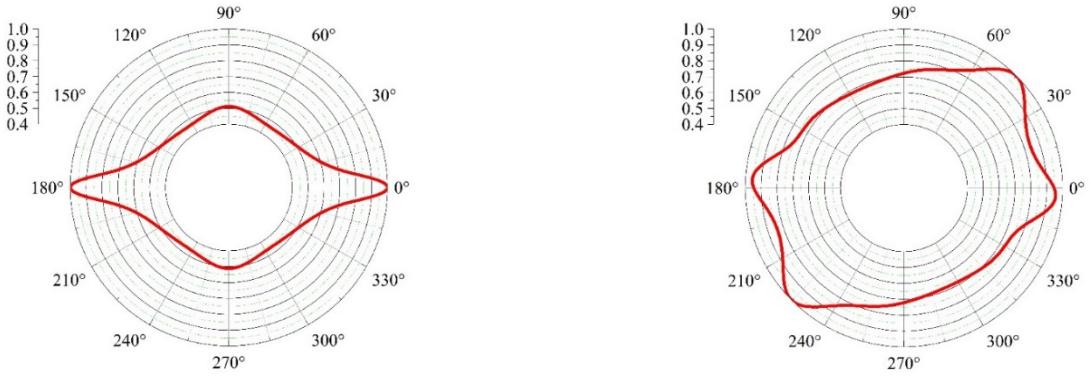

(a) [0°,0°] (b) [0°,45°]

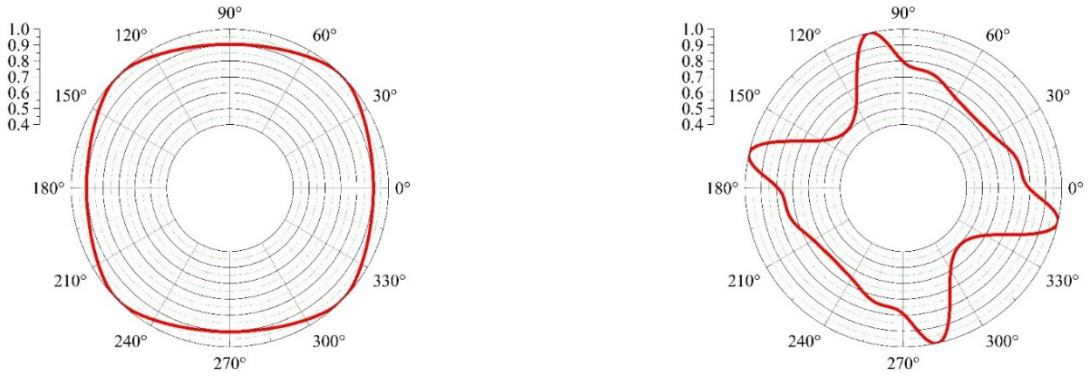

(c) [-45°,45°] (d) [0°,45°,90°]

Fig. 4 — Normalized amplitude of elastic waves in different directions of composite plates

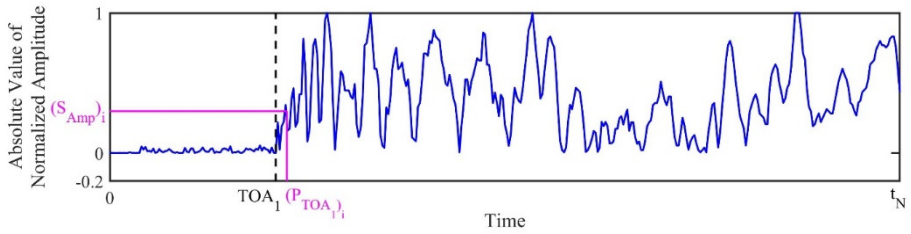

(a) S1

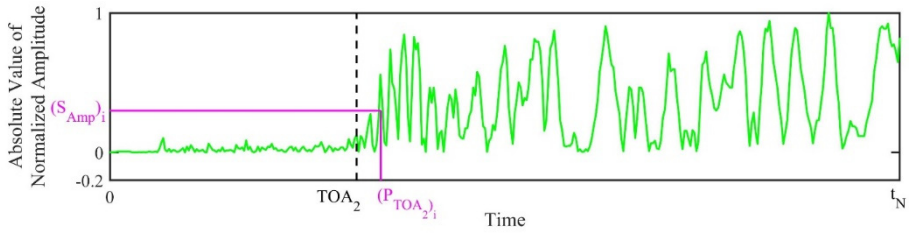

(b) S2

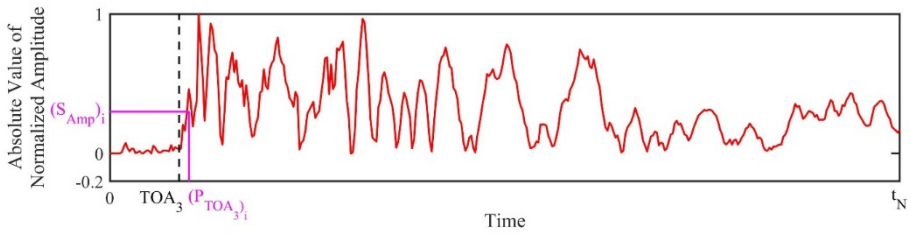

(c) S3

Fig. 5 Typical estimated time of arrival of signal collected by sensor

normalize the amplitude of each signal by its maximum value.

The second step is to determine the absolute value of the signal. Then, the times at which the amplitude of each signal reaches to a specific amplitude, $(S_{\text{Amp}})_i$ can be considered as the estimated time of arrival $(P_{\text{TOA}})_i$ of that signal (see Fig. 5).

The specific amplitude $(S_{\text{Amp}})_i$, can be chosen between zero to one. Since, different specific amplitude values result in different estimated time of arrivals, for each signal, a number of N specific amplitude values are chosen between $(S_{\text{Amp}})_1$ and $(S_{\text{Amp}})_N$ with a step of $\Delta\beta$. Therefore

$$(S_{\text{Amp}})_i = (S_{\text{Amp}})_1 + [(i \times \Delta\beta) - \Delta\beta], \quad i = 1,2,\dots,N \quad (3)$$

where $(S_{\text{Amp}})_1$ and $(S_{\text{Amp}})_N$ are respectively, the initial and threshold specific amplitude values.

For each specific amplitude value, the estimated time of arrival of each signal is determined. The actual TOAs in Eq. (2) are substituted by the estimated time of arrivals.

However, since the estimated TOAs are approximately (not exactly) equal to the actual TOAs, Eq. (2) results in residual value.

Hence, for each pair of signals, a residual value can be determined as follow

$$\sum_{i=1}^{N}\left|L_{I-S1} - \left[L_{I-S2} \times \left(\frac{V_{\theta_{I-S1}}}{V_{\theta_{I-S2}}} \times \frac{(P_{TOA_1})_i}{(P_{TOA_2})_i}\right)\right]\right| = r_{12} \quad (4a)$$

$$\sum_{i=1}^{N}\left|L_{I-S1} - \left[L_{I-S3} \times \left(\frac{V_{\theta_{I-S1}}}{V_{\theta_{I-S3}}} \times \frac{(P_{TOA_1})_i}{(P_{TOA_3})_i}\right)\right]\right| = r_{12} \quad (4b)$$

$$\sum_{i=1}^{N}\left|L_{I-S2} - \left[L_{I-S3} \times \left(\frac{V_{\theta_{I-S2}}}{V_{\theta_{I-S3}}} \times \frac{(P_{TOA_2})_i}{(P_{TOA_3})_i}\right)\right]\right| = r_{23} \quad (4c)$$

where, r_{12}, r_{13}, and r_{23}, are the residual value of respectively sensor pairs S1&S2, S1&S3, and S2&S3.

In order to calculate the residual value, as can be seen in Eq. (4), we need the distances between the impact point and different sensors ($L_{\text{I-S1}}$, $L_{\text{I-S2}}$, and $L_{\text{I-S3}}$). However, since the location of the impact point I is unknown, these distances are also unknown. To overcome this obstacle, the composite plate is meshed into uniformly grid points (see Fig. 6).

We imagine that the grid point G_i is the actual location of impact. Now, the distances between this grid point and different sensors (for example, L_{G_i-S1}, L_{G_i-S2}, and L_{G_i-S3}) can be determined. By substituting them into Eq. (4), the residual value can be determined as follow

$$\sum_{i=1}^{N}\left|L_{G_i-S1} - \left[L_{G_i-S2} \times \left(\frac{V_{\theta_{G_i-S1}}}{V_{\theta_{G_i-S2}}} \times \frac{(P_{TOA_1})_i}{(P_{TOA_2})_i}\right)\right]\right| = r_{12} \quad (5a)$$

$$\sum_{i=1}^{N}\left|L_{G_i-S1} - \left[L_{G_i-S3} \times \left(\frac{V_{\theta_{G_i-S1}}}{V_{\theta_{G_i-S3}}} \times \frac{(P_{TOA_1})_i}{(P_{TOA_3})_i}\right)\right]\right| = r_{13} \quad (5b)$$

$$\sum_{i=1}^{N}\left|L_{G_i-S2} - \left[L_{G_i-S3} \times \left(\frac{V_{\theta_{G_i-S}}}{V_{\theta_{G_i-S3}}} \times \frac{(P_{TOA_2})_i}{(P_{TOA_3})_i}\right)\right]\right| = r_{23} \quad (5c)$$

The summation of all residual values, gives the total residual value of the grid point G_i as follow

$$r_{G_i} = r_{12} + r_{13} + r_{23} + \dots \quad (6)$$

where, r_{G_i} is the total residual value of the grid point G_i. This process is repeated for each grid point and the total residual value of all grid points are calculated.

Depends on the location of each grid point, the amount of residual value can be different. In fact, there are three factors which affect the residual value including

i. The difference between the estimated TOAs and the actual TOAs (for all grid points)
ii. Incompatibility between the estimated TOAs and the distances between the grid point and different sensors (for those grid points which are not the actual location of impact)
iii. Selecting wrong wave velocities (for those grid points which are not the actual location of impact)

As is mentioned above, for the grid point which is the exact location of impact, there is only one source of residual value which is the difference between the actual TOAs and the estimated TOAs. But, for the other grid points, in addition to this source, there are two more sources including the incompatibility between the estimated TOAs and the distances between the grid point and different sensors, and also selecting wrong wave velocities. This of course, increases the amount of total residual value in these grid points. Hence, the total residual value at the impact location will be less than other grid points. Therefore, the grid point with the minimum total residual value highlights the most probable location of impact.

3. Experimental setup

The performance of the developed impact localization technique was experimentally evaluated by impact tests on a carbon fibre composite plate $[0°, 90°, 0°, 90°]_S$ of dimensions 800 mm × 800 mm with 1 mm thickness. For signal collection, 25 APC 851 piezoelectric sensors were attached to the plate using epoxy (see Fig. 7(a)). Three cases of impacts were used. In case one, a steel ball with 1.5 cm diameter from the height of 1 m was dropped on point I1, in case two, a steel ball with 2 cm diameter from the height of 2 m was dropped on point I2, and in case three, a steel ball with 3 cm diameter from the height of 2 m was dropped on point I3 (see Fig. 7(b)).

In order to drop steel balls from correct height and right on the assigned point, pipes with different lengths were used (see Fig. 8(a)).

A Vantage 32 LE system was used for signal collection (see Fig. 8(b)). Signals were collected at 0.5 M samples/second for a time duration of 1 ms. In order to evaluate the performance of the proposed method in the

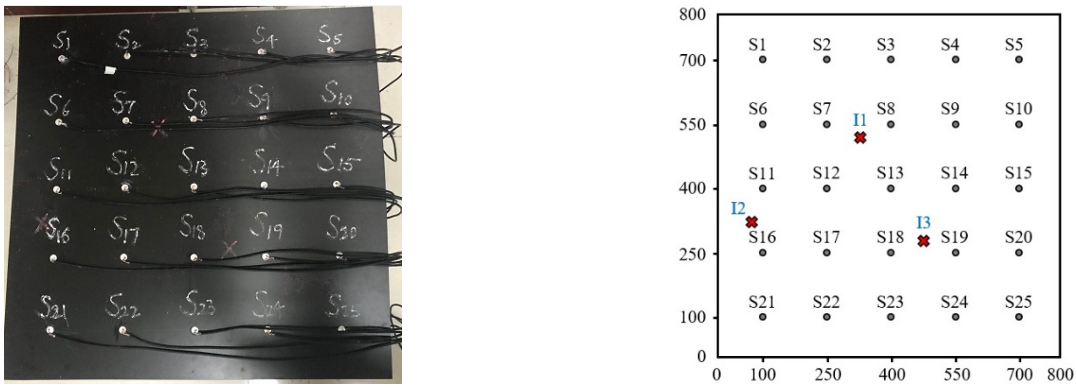

(a) (b)

Fig. 7 (a) carbon fiber composite plate $[0°, 90°, 0°, 90°]_S$ with 25 bonded PZT sensors; (b) actual location of impact points I1(325,520), I2(80,325), and I3(475,270) (dimensions in mm)

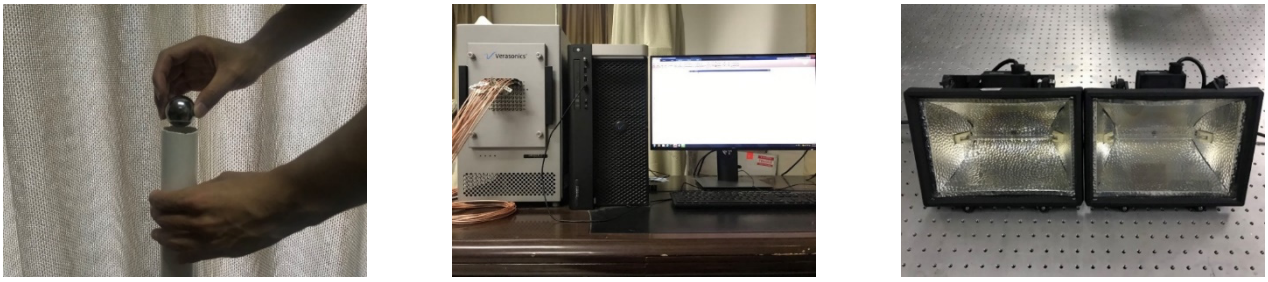

(a) (b) (c)

Fig. 8 (a) Dropping steel balls through pipes; (b) Vantage 32 LE; (c) Halogen Lamps for temperature fluctuation

presence of temperature fluctuations, the temperature of the plate was increased by using two Halogen Lamps (see Fig. 8(c)) at each side of the plate. Whilst, the temperature distribution in the plate were not completely uniform, nevertheless, the temperature difference in different regions of the plate was less than 2°C.

4. Results and discussion

4.1 Normalized wave velocity determination

The first step for impact localization on the carbon fibre composite plate $[0°, 90°, 0°, 90°]_S$ is to determine the wave velocity in different directions. To this aim, a finite element model of the plate was built in ABAQUS/CAE. The plate was modeled as 3D deformable shell.

The plate was fixed at periphery with "ENCASTRE" boundary condition available in the code to restrict all degrees of freedom.

The plate was meshed with S4R elements (4-node doubly curved thin or thick shell, reduced integration, hourglass control) available in the code. Since, the changes in wave velocity in different directions only depends on the material properties of the plate, and also since only the normalized wave velocities are required, any type of wave at favorable frequency can be used in the analysis. Therefore, a five burst Lamb wave with a central frequency

(a) Oblique view (b) Top view

Fig. 9 Displacement of the propagated waves on the carbon fibre composite plate $[0°, 90°, 0°, 90°]_S$

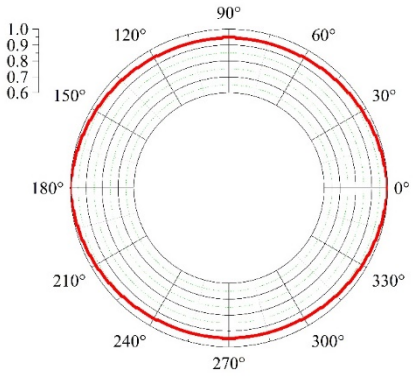

Fig. 10 Normalized amplitude of waves in different directions of the carbon fibre composite plate $[0°, 90°, 0°, 90°]_S$

of 200 kHz was generated at the center of plate using ABAQUS/Implicit. The propagated wave on the plate is demonstrated in Fig. 9.

The displacement of all nodes located on a circumference of a circle with the centre of plate and radius of 100 mm were obtained. The envelope of all signals was determined and based on the peak time, the velocity of propagated waves at different directions was calculated. Fig. 10 shows the normalized wave velocity at different directions.

These numerically determined normalized wave velocity values were used in experimentally impact localization process.

4.2 The efficiency of the developed technique

The effectiveness of the presented method was first checked for impact case one. Fig. 11 shows typical captured signals.

The absolute value of the normalized signals was determined and by choosing 10 specific amplitude values between $\left(S_{\mathrm{Amp}}\right)_1 = 0.1$ and $\left(S_{\mathrm{Amp}}\right)_N = 1$ with a step of $\Delta\beta = 0.1$, 10 estimated TOAs were determined for each signal. Fig. 12 shows the estimated TOAs of typical signals, for the specific amplitude values of 0.1, 0.4, and 0.9.

As can be seen in Fig. 12, if the initial specific amplitude value be chosen close to zero, the TOA estimation procedure may be influenced by noise and results in false estimated TOA. Moreover, if the threshold specific amplitude value be chosen close to one, the TOA estimation procedure may be influenced by the intersection of boundaries reflections with amplitude higher than direct waves, and results in false estimated TOA. However, for other specific amplitude values, as can be seen in Figs. 11 and 12, the estimated TOAs are close to the actual TOAs.

Then, by dividing each side of the plate into 80 segments, the plate was meshed into 6561 grid points. Using the procedure introduced in section 2, the total residual value at each grid point was calculated and is shown in Fig. 13.

It can be seen in Fig. 13, that the grid point with the minimum residual value is close to the actual impact

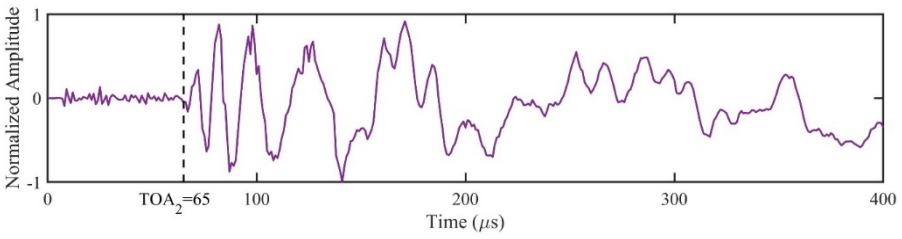

(a) S2

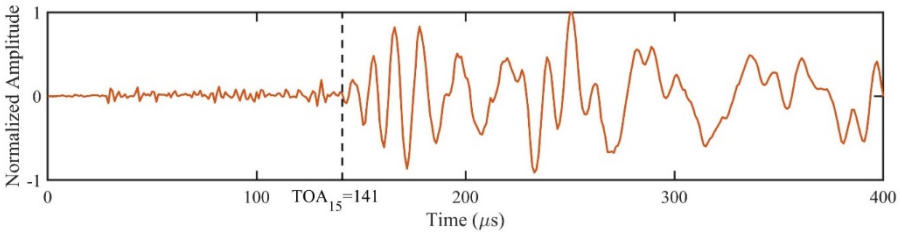

(b) S15

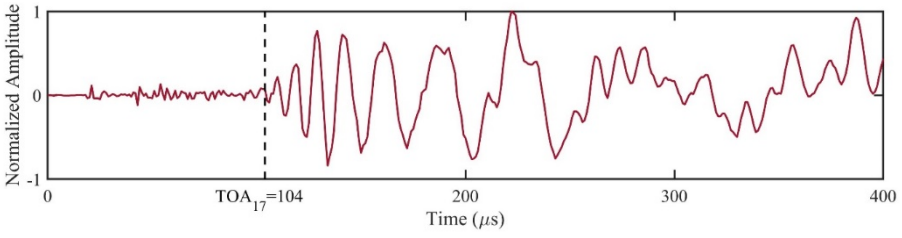

(c) S17

Fig. 11 Typical captured signals in the first impact case by sensors

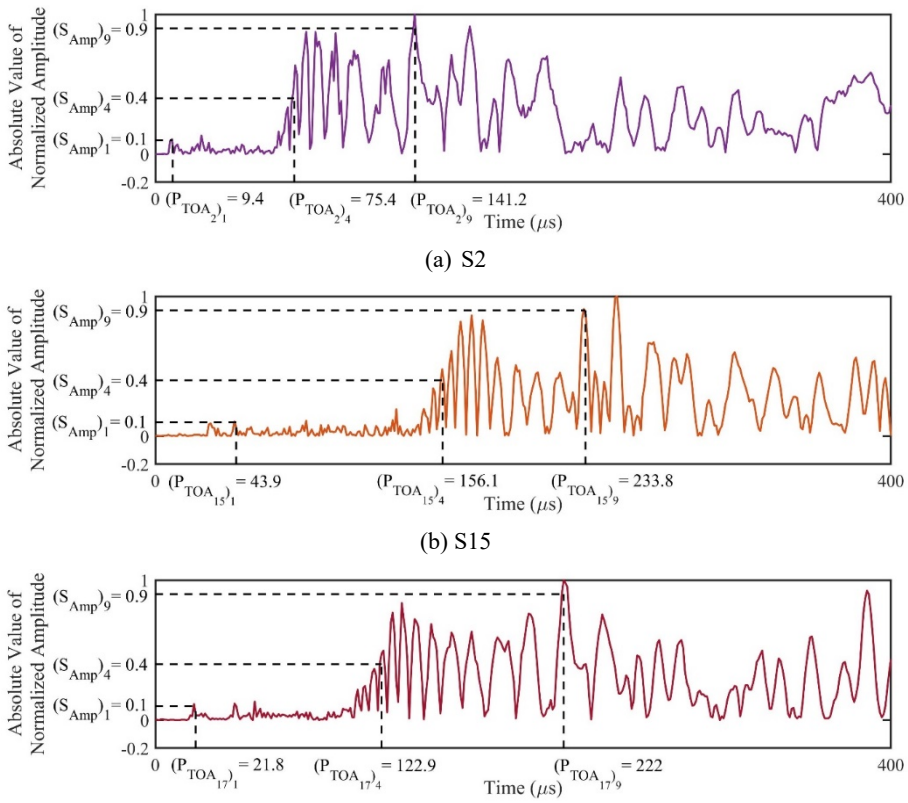

(a) S2

(b) S15

(c) S17

Fig. 12 Normalized amplitude of captured signals for the impact case one by sensors

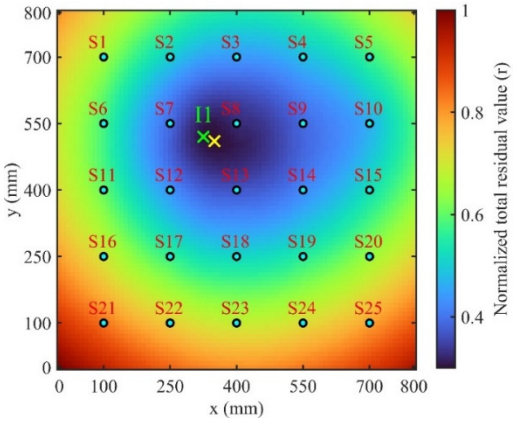

Fig. 13 Normalized total residual value at different grid points (green and yellow crosses respectively demonstrate the actual impact point and the grid point with the minimum total residual value)

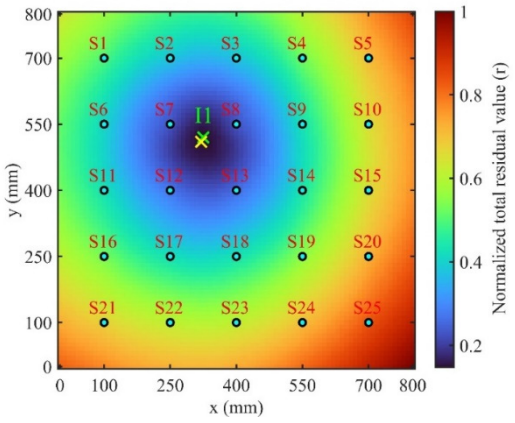

Fig. 14 Normalized total residual value of grid points by using the specific amplitude values between $(S_{\mathrm{Amp}})_1 = 0.2$ and $(S_{\mathrm{Amp}})_N = 0.8$ with a step of $\Delta\beta = 0.1$, (green and yellow crosses respectively demonstrate the actual impact point and the grid point with the minimum total residual value)

location and shows the effectiveness of the developed method for impact localization in composite plates.

4.3 Effect of specific amplitude

As is mentioned above, for the initial specific amplitude value close to zero, the TOA estimation procedure may be influenced by noise and results in false estimated TOA. On the other hand, for the threshold specific amplitude value close to one, the TOA estimation procedure may be affected by intersection of boundaries reflections with amplitude higher than direct waves, and results in false estimated TOA.

In order to evaluate the effect of specific amplitude range on the performance of the developed method, the procedure was once again repeated but this time only $N = 7$ specific amplitude values between $(S_{\mathrm{Amp}})_1 = 0.2$ and

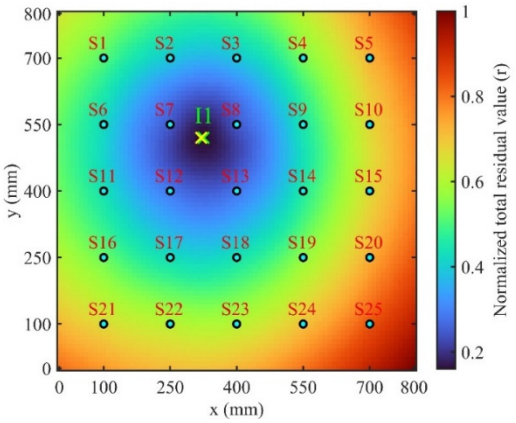

Fig. 15 Normalized total residual value at different grid points by using the specific amplitude values between $(S_{\mathrm{Amp}})_1 = 0.2$ and $(S_{\mathrm{Amp}})_N = 0.8$ with a step of $\Delta\beta = 0.025$, (green and yellow crosses respectively demonstrate the actual impact point and the grid point with the minimum total residual value)

$(S_{\mathrm{Amp}})_N = 0.8$ with a step of $\Delta\beta = 0.1$, were used in the procedure. The total residual value of all grid points was determined and is shown in Fig. 14.

By comparing Figs. 13 and 14, it can be figured out that omitting specific amplitude values close to zero and one, leads to enhancing the accuracy of the proposed impact localization procedure.

The other parameter which may influence the performance of the proposed impact localization method is the number of specific amplitude values N, or in other words the step value ($\Delta\beta$). To check this, the procedure was once again repeated but this time $N = 25$ specific amplitude values between $(S_{\mathrm{Amp}})_1 = 0.2$ and $(S_{\mathrm{Amp}})_N = 0.8$ with a step of $\Delta\beta = 0.025$, were used. The total residual value of all grid points was determined and is demonstrated in Fig. 15.

By comparing Figs. 14 and 15 it can be figured out that using more specific amplitude values increases the efficiency of the developed impact localization method.

4.4 Effect of measurement noise

In order to assess the efficiency of the proposed technique in the presence of noise, a Gaussian white noise was added to all captured signals. The noise to signal ratio was chosen 10%. Fig. 16 shows typical corrupted signals.

By choosing $N = 21$ specific amplitude values between $(S_{\mathrm{Amp}})_1 = 0.3$ and $(S_{\mathrm{Amp}})_N = 0.8$ with a step of $\Delta\beta = 0.025$, the total residual value of all grid points was determined and is shown in Fig. 17.

As can be seen in Fig. 17, the grid point with the minimum total residual value is very close to the actual location of impact. This shows that by choosing

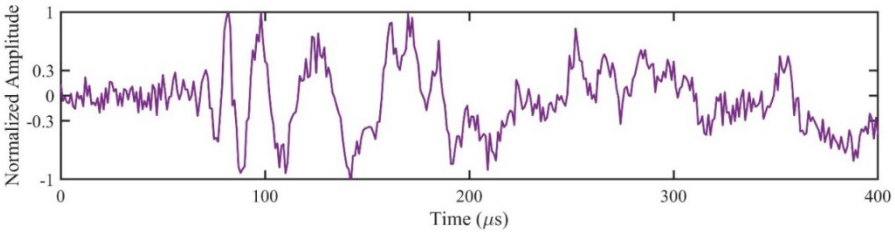

(a) S2

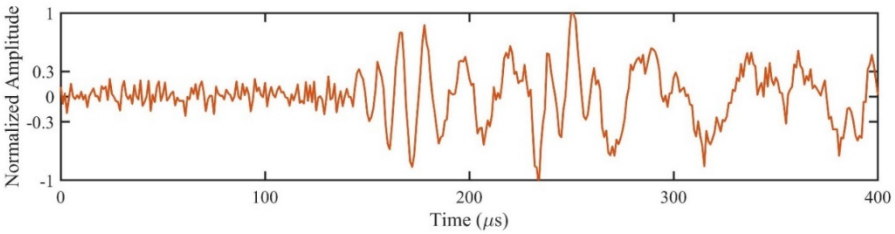

(b) S15

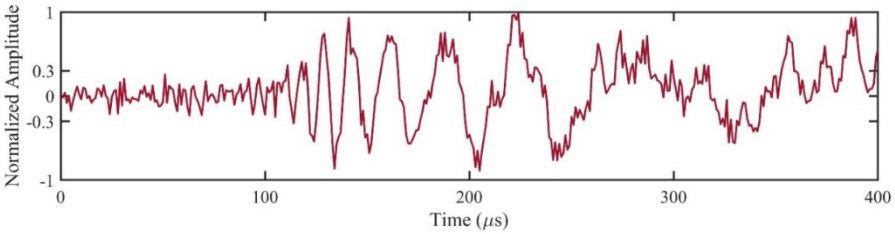

(c) S17

Fig. 16 Typical corrupted signals collected by sensors

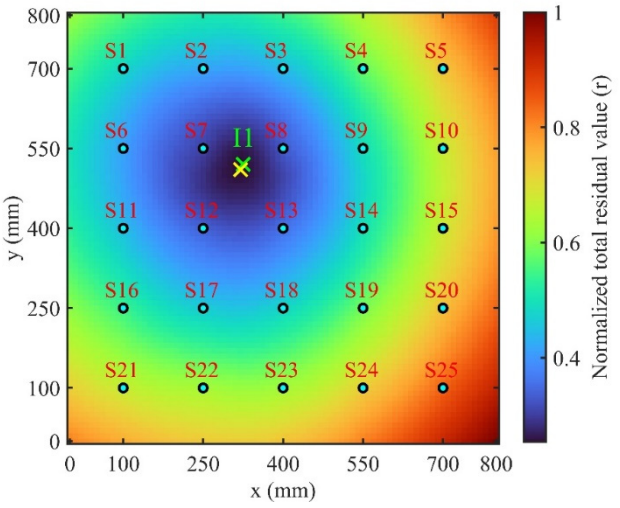

Fig. 17 Normalized total residual value at different grid points for corrupted signals by using the specific amplitude values between $\left(S_{\text{Amp}}\right)_1 = 0.3$ and $\left(S_{\text{Amp}}\right)_N = 0.8$ with a step of $\Delta\beta = 0.025$, (green and yellow crosses respectively demonstrate the actual impact point and the grid point with the minimum total residual value)

an appropriate value for the minimum specific amplitude value, the effect of measurement noise can be compensated.

4.5 Impacts with different energies and locations

In order to check the efficiency of the developed technique in localizing impacts with different energies and locations, the proposed method was once again used for impact cases two and three.

In impact case two, a steel ball with 2 cm diameter from the height of 2 m was dropped on impact point I2. Elastic waves were collected by PZT sensors. Then, by choosing $N = 25$ specific amplitude values between $\left(S_{\text{Amp}}\right)_1 = 0.2$ and $\left(S_{\text{Amp}}\right)_N = 0.8$ with a step of $\Delta\beta = 0.025$, the total residual value at each grid point was calculated and is shown in Fig. 18(a). In case three, a steel ball with 3 cm diameter from the height of 2 m was dropped on impact point I3. Using the developed procedure, the total residual value at each grid point of the composite plate was calculated and is shown in Fig. 18(b). As can be seen in Figs. 18 and 15, the developed method is able to localize impacts with different energies and locations.

4.6 Effect of temperature fluctuations

To assess the influence of temperature fluctuation on the presented method, the impact cases one to three were repeated in 55°C. Fig. 19 demonstrates the signals acquired by sensor S2 in 25°C and 55°C due to impact case one.

As can be seen in Fig. 19, temperature variation caused changes in the amplitude and phase of the elastic waves. Using the developed procedure, the total residual value in

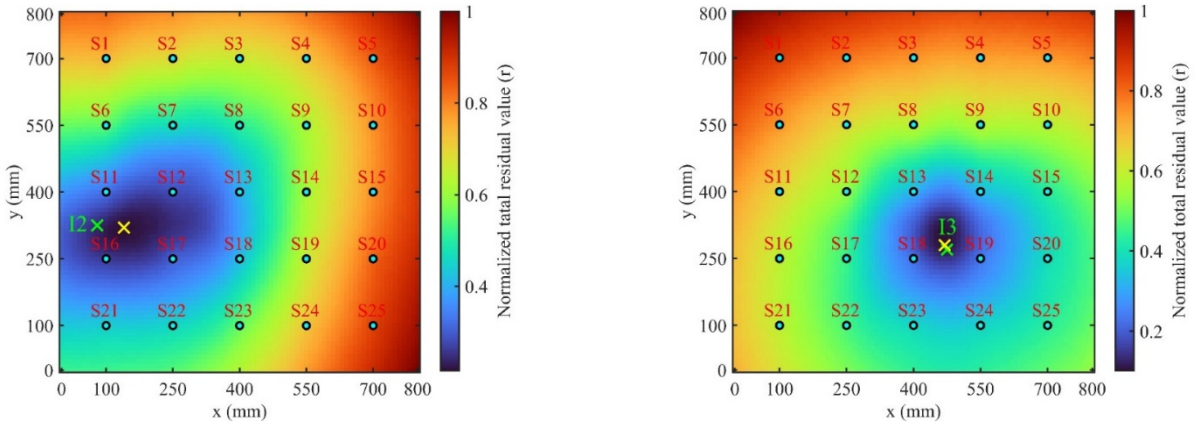

(a) (b)

Fig. 18 Normalized total residual value at different grid points for; (a) case two, (b) case three, (green and yellow crosses respectively demonstrate the actual impact point and the grid point with the minimum total residual value)

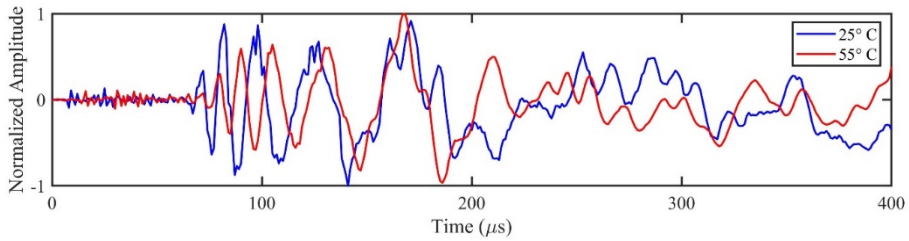

Fig. 19 Signals acquired by sensor S2 in 25°C and 55°C due to impact case one

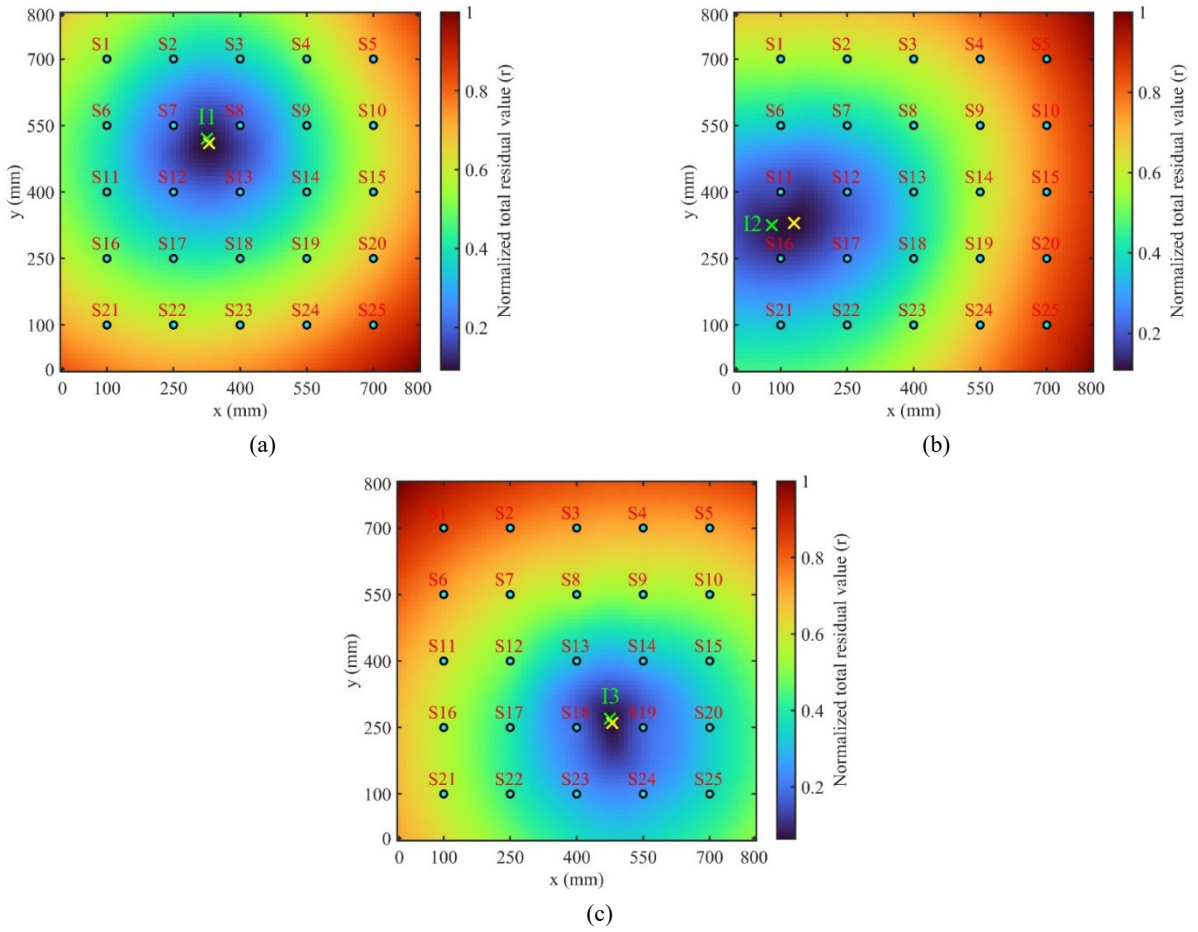

(a) (b)

(c)

Fig. 20 Normalized total residual value at different grid points for tests conducted in 55°C; (a) case one; (b) case two; (c) case three (green and yellow crosses respectively demonstrate the actual impact point and the grid point with the minimum total residual value)

each grid point is calculated for all three impact cases in 55°C and shown in Fig. 20.

By comparing Fig. 20 with Figs. 15 and 18, it can be figured out that temperature fluctuation doesn't have a significant influence on the efficiency of the proposed technique. This is firstly because, changes in amplitude of signals due to temperature fluctuation can be compensated by normalising signals. Secondly, the ratio of the estimated TOAs is appeared in Eq. (5), any changes in the phase of signals will not have a significant effect on the performance of the presented method. Therefore, the proposed technique remains effective even in the presence of temperature fluctuations.

4.7 Effect of using low dense sensor network

In order to evaluate the efficiency of the proposed method when a low dense sensor network is available, the impact localization process was repeated for the impact case 3, but this time only 9 signals, captured by sensors S1, S3, S5, S11, S13, S15, S21, S23, and S25 were used.

By choosing $N = 25$ specific amplitude values between $\left(S_{\mathrm{Amp}}\right)_1 = 0.2$ and $\left(S_{\mathrm{Amp}}\right)_N = 0.8$ with a step of $\Delta\beta = 0.025$, the total residual value of all grid points was determined and is shown in Fig. 21.

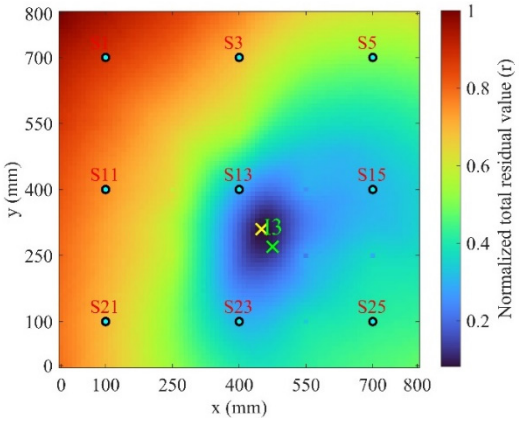

Fig. 21 Normalized total residual value at different grid points for impact case 3 using a low dense sensor network (green and yellow crosses respectively demonstrate the actual impact point and the grid point with the minimum total residual value)

By comparing Fig. 21 with Fig. 18(b), it can be found out that when a low dense sensor network is used the accuracy of proposed method decreases to some extent. However, the grid point with the minimum residual value is

still close to the actual impact location which shows the effectiveness of the developed method even when a low dense sensor network be used.

5. Conclusions

This study presented an impact localization technique for composite structures. Since, the proposed method required the normalized wave velocities of elastic waves in all directions of propagation, a finite element model of the plate was built in ABAQUS/CAE. It was shown that the normalized wave velocities can be determined by generating a five burst Lamb wave at any frequency. Then, a robust TOA estimation technique was developed based on the amplitude of the acquired signals. It was demonstrated that the time in which the amplitude of a signal becomes equal to a specific amplitude value, can be chosen as the estimated TOA of that signal. The presented TOA estimation technique didn't require any sophisticated signal processing, make it attractive for real-time impact localization systems. It was also demonstrated that choosing a suitable initial and threshold for specific amplitude values and also increasing the number of specific amplitude values, enhance the accuracy of the presented method. Several tests conducted on a carbon fiber composite plate at two different temperatures, demonstrated that the presented technique is able to localize impacts with different energies at different locations of the plate even in the presence of noise, temperature fluctuations or using low dense sensor network.

Acknowledgments

This work was financially supported by the National Natural Science Foundation of China (11872191).

References

Boschetti, F., Dentith, M.D. and List, R.D. (1996), "A fractal-based algorithm for detecting first arrivals on seismic traces", *Geophysics*, **61**(4), 1095-1102. https://doi.org/10.1190/1.1444030

Ciampa, F. and Meo, M. (2010a), "Acoustic emission source localization and velocity determination of the fundamental mode A0 using wavelet analysis and a Newton-based optimization technique", *Smart Mater. Struct.*, **19**(4), 045027. https://doi.org/10.1088/0964-1726/19/4/045027

Ciampa, F. and Meo, M. (2010b), "A new algorithm for acoustic emission localization and flexural group velocity determination in anisotropic structures", *Compos. Part A: Appl. Sci. Manuf.*, **41**(12), 1777-1786. https://doi.org/10.1016/j.compositesa.2010.08.013

Ciampa, F., Meo, M. and Barbieri, E. (2012), "Impact localization in composite structures of arbitrary cross section", *Struct. Health Monitor.*, **11**(6), 643-655. https://doi.org/10.1177/1475921712451951

Coverley, P.T. and Staszewski, W.J. (2003), "Impact damage location in composite structures using optimized sensor triangulation procedure", *Smart Mater. Struct.*, **12**(5), 795-803. https://doi.org/10.1088/0964-1726/12/5/017

De Simone, M.E., Ciampa, F., Boccardi, S. and Meo, M. (2017), "Impact source localisation in aerospace composite structures" *Smart Mater. Struct.*, **26**(12), 125026. https://doi.org/10.1088/1361-665X/aa973e

Farrar, C.R. and Worden, K. (2006), "An introduction to structural health monitoring", *Philosoph. Transact. Royal Soc. A, Mathe. Phys. Eng. Sci.*, **365**(1851), 303-315. https://doi.org/10.1098/rsta.2006.1928

Gorgin, R. and Wang, Z. (2021), "Baseline-free damage imaging technique for Lamb wave based structural health monitoring systems", *Smart Struct. Syst., Int. J.*, **28**(5), 689-698. https://doi.org/10.12989/sss.2021.28.5.689

Gorgin, R., Wang, Y., Gao, D. and Wu, Z. (2015), "Probabilistic-based damage identification based on error functions with an autofocusing feature", *Smart Struct. Syst., Int. J.*, **15**(4), 1121-1137. https://doi.org/10.12989/sss.2015.15.4.1121

Gorgin, R., Luo, Y. and Wu, Z. (2020), "Environmental and operational conditions effects on Lamb wave based structural health monitoring systems: A review", *Ultrasonics*, **105**, 106114. https://doi.org/10.1016/j.ultras.2020.106114

He, T., Pan, Q., Liu, Y., Liu, X. and Hu, D. (2012), "Near-field beamforming analysis for acoustic emission source localization", *Ultrasonics*, **52**(5), 587-592. https://doi.org/10.1016/j.ultras.2011.12.003

Hinkley, D.V. (1971), "Inference about the change-point from cumulative sum tests", *Biometrika*, **58**, 509-523. https://doi.org/10.1093/biomet/58.3.509

Huynh, T-C. and Kim, J-T. (2016), "Compensation of temperature effect on impedance responses of PZT interface for prestress-loss monitoring in PSC girders", *Smart Struct. Syst., Int. J.*, **17**(6), 881-901. https://doi.org/10.12989/sss.2016.17.6.881

Jang, B-W. and Kim, C-G. (2016), "Impact localization on a composite stiffened panel using reference signals with efficient training process", *Compos. Part B: Eng.*, **94**, 271-285. https://doi.org/10.1016/j.compositesb.2016.03.063

Jang, B-W. and Kim, C-G. (2019), "Impact localization of composite stiffened panel with triangulation method using normalized magnitudes of fiber optic sensor signals", *Compos. Struct.*, **211**, 522-529. https://doi.org/10.1016/j.compstruct.2019.01.028

Jang, B-W., Lee, Y-G., Kim, J-H., Kim, Y-Y. and Kim, C-G. (2012), "Real-time impact identification algorithm for composite structures using fiber Bragg grating sensors", *Struct. Control Health Monitor.*, **19**(7), 580-591. https://doi.org/10.1002/stc.1492

Kim, J-H., Kim, Y-Y., Park, Y. and Kim, C-G. (2015), "Low-velocity impact localization in a stiffened composite panel using a normalized cross-correlation method", *Smart Mater. Struct.*, **24**, 045036. https://doi.org/10.1088/0964-1726/24/4/045036

Kosel, T., Grabec, I. and Kosel, F. (2003), "Intelligent location of simultaneously active acoustic emission sources: part 1", *Aircr. Eng. Aerosp. Technol.*, **75**(1), 11-17. https://doi.org/10.1108/00022660310457248

Kundu, T., Das, S. and Jata, K.V. (2007), "Point of impact prediction in isotropic and anisotropic plates from the acoustic emission data", *J. Acoust. Soc. Am.*, **122**, 2057-2066. https://doi.org/10.1121/1.2775322

Kundu, T., Das, S., Martin, S.A. and Jata, K.V. (2008), "Locating point of impact in anisotropic fiber reinforced composite plates", *Ultrasonics*, **48**(3), 193-201. https://doi.org/10.1016/j.ultras.2007.12.001

McLaskey, G.C., Glaser, S.D. and Grosse, C.U. (2010), "Beamforming array techniques for acoustic emission monitoring of large concrete structures", *J. Sound Vib.*, **329**(12), 2384-2394. https://doi.org/10.1016/j.jsv.2009.08.037

Nakatani, H., Hajzargarbashi, T., Ito, K., Kundu, T. and Nobuo, T. (2013), "Locating point of impact on an anisotropic cylindrical

surface using acoustic beamforming technique", *Key Eng. Mater.*, **558**, 331-340. https://doi.org/10.4028/www.scientific.net/KEM.558.331

Park, B., Sohn, H., Olson, S.E., DeSimio, M.P., Brown, K.S. and Derriso, M.M. (2012), "Impact localization in complex structures using laser-based time reversal", *Struct. Health Monitor.*, **11**(5), 577-588. https://doi.org/10.1177/1475921712449508

Qiu, L., Deng, X., Yuan, S., Huang, Y. and Ren, Y. (2018), 'Impact monitoring for aircraft smart composite skins based on a lightweight sensor network and characteristic digital sequences", *Sensors*, **18**(7), 2218. https://doi.org/10.3390/s18072218

Seno, A.H. and Aliabadi, M.H. (2019), "Impact localisation in composite plates of different stiffness impactors under simulated environmental and operational conditions", *Sensors*, **19**(17), 3659. https://doi.org/10.3390/s19173659

Seno, A.H. and Aliabadi, M.H. (2022), "Uncertainty quantification for impact location and force estimation in composite structures", *Struct. Health Monitor.*, **21**(3). https://doi.org/10.1177/14759217211020255

Sharif Khodaei, Z., Ghajari, M. and Aliabadi, M.H. (2012), "Determination of impact location on composite stiffened panels", *Smart Mater. Struct.*, **21**(10), 105026. https://doi.org/10.1088/0964-1726/21/10/105026

Shrestha, P., Park, Y. and Kim, C-G. (2017), "Low velocity impact localization on composite wing structure using error outlier based algorithm and FBG sensors", *Compos. Part B: Eng.*, **116**, 298-312. https://doi.org/10.1016/j.compositesb.2016.10.068

Xu, J. (2011), "P-wave onset detection based on the spectrograms of the AE signals", *Adv. Mater. Res.*, **250**, 3807-3810. https://doi.org/10.4028/www.scientific.net/AMR.250-253.3807

Yue, N. and Sharif Khodaei, Z. (2016), "Assessment of impact detection techniques for aeronautical application: ANN vs LSSVM", *J. Multisc. Modell.*, **7**(4), 1640005. https://doi.org/10.1142/S1756973716400059

Zhao, G., Li, S., Hu, H., Zhong, Y. and Li, K. (2018), "Impact localization on composite laminates using fiber Bragg grating sensors and a novel technique based on strain amplitude", *Optical Fiber Technol.*, **40**, 172-179. https://doi.org/10.1016/j.yofte.2017.12.001

Zhong, Y. and Xiang, J. (2019), "Impact location on a stiffened composite panel using improved linear array", *Smart Struct. Syst., Int. J.*, **24**(2), 173-182. https://doi.org/10.12989/sss.2019.24.2.173

Ziola, S.M. and Gorman, M.R. (1991), "Source location in thin plates using cross-correlation", *J. Acoust. Soc. Am.*, **90**(5), 2551-2556. https://doi.org/10.1121/1.402348

HJ